Materials Today Physics 35 (2023) 101090

Contents lists available at ScienceDirect

Materials Today Physics

journal homepage: www.journals.elsevier.com/materials-today-physics

Matryoshka-inspired continuous assembly of flexible silicon microribbons and photodetectors via selective transfer printing

Chunyan Qu [a,c,d], Qinglei Guo [e,*], Xiaozhong Wu [e], Chunyu You [a,c,d], Binmin Wu [a,c,d], Ziyu Zhang [a,c,d], Yongfeng Mei [a,b,c,d,**]

[a] Department of Materials Science & State Key Laboratory of Molecular Engineering of Polymers, Fudan University, Shanghai, 200438, People's Republic of China
[b] Shanghai Frontiers Science Research Base of Intelligent Optoelectronics and Perception, Institute of Optoelectronics, Fudan University, Shanghai, 200438, People's Republic of China
[c] International Institute of Intelligent Nanorobots and Nanosystems, Fudan University, Shanghai, 200438, People's Republic of China
[d] Yiwu Research Institute of Fudan University, Yiwu, 322000, Zhejiang, People's Republic of China
[e] School of Microelectronics, Shandong University, Jinan, 250100, Shandong, People's Republic of China

ARTICLE INFO

Keywords:
Silicon microribbons
Selective transfer printing
Deterministic assembly
Flexible electronics
Photodetectors

ABSTRACT

Silicon microribbon (SiMR), as an intermediate structure format between silicon nanowire and silicon nanomembrane, is of great interest to serve as the functional material for flexible electronics, which represents an unusual electronic platform with widespread applications and promising future. However, the scalable production of SiMRs and/or devices on flexible substrates, in a deterministic assembly manner, still faces significant challenges. Herein, inspired by the matryoshka doll, referring to a set of dolls with decreased size and placed one inside another, we develop a universal and convenient approach to continuously and deterministically assemble flexible SiMRs and electronic devices through the selective transfer printing technique. By optimizing and repeating the selective transfer printing, continuous assembly of flexible SiMRs and devices are realized. Both theoretical calculation and simulation are performed to analyze the influence of the utilized viscoelastic stamp on the adhesive energy with SiMR, thus providing guidance for optimizing the design of stamp microstructure and enhancing the transfer efficiency of SiMRs. Finally, matryoshka-like flexible photodetectors, as an example, are fabricated by utilizing the sequentially prepared SiMRs via the proposed approach. This matryoshka-inspired assembly approach can be extended to prepare other functional semiconducting microribbons or devices in high controllability and yield, thus implying a promising future in the field of flexible electronics.

1. Introduction

Low-dimensional semiconducting materials, such as quasi-0D [1,2], 1D and quasi-1D [3,4], 2D and quasi-2D [5,6], usually offer extraordinary electronic, optical, thermal, mechanical, and chemical properties that cannot be reproduced in other material formats, and of importance to the expanding frontiers in nanoscience and technology [7–9]. Common low-dimensional structures include quantum dots [10], tubes [11], wires [12], rods [13], ribbons [14], sheets [15], membranes [16], core/shell structures [17], and other related. Among them, semiconducting microribbons have drawn great attentions due to their widespread applications in sensing devices such as photodetectors [18–20], biosensors [21,22], electrochemical sensors [23], energy harvesting and storage devices [24–26], 3D structures self-assembly [27,28], and stretchable electronics [29,30]. Compared with 0D and 1D structures, semiconducting microribbons can be more compatible with available microfabrication techniques, thus facilitating the fabrication of electronic device with various functionalities [31]. However, significant challenges exist in terms of production and deterministic assembly of these semiconducting microribbons (about 1 μm in width) [32,33].

Promising results can be obtained via precise patterning and etching of the donor materials via high-resolution lithographic processing [21,34], such as electron beam lithography (EBL) [35,36] and focused-ion-beam (FIB) [37,38], although they are not suitable for

* Corresponding author.
** Corresponding author. Department of Materials Science & State Key Laboratory of Molecular Engineering of Polymers, Fudan University, Shanghai, 200438, People's Republic of China.
E-mail addresses: qlguo@sdu.edu.cn (Q. Guo), yfm@fudan.edu.cn (Y. Mei).

https://doi.org/10.1016/j.mtphys.2023.101090
Received 16 February 2023; Received in revised form 3 April 2023; Accepted 17 April 2023
Available online 8 June 2023

large-scale production [39]. Nanoimprint lithography (NIL) [40,41] provide the possibility for large-scale production, while the molds fabrication still requires high-resolution lithographic processing [42]. Moreover, the following deterministic assembly of the produced semiconducting microribbons on flexible substrates, which is known as the key step for the manufacturing of flexible electronics, especially for those in sub-micrometer scale, is also highly demanded. Besides, traditional patterning and etching processes need to remove the undemand parts from the donor, which even worse for the fabrication of semiconducting microribbons and devices, thus causing the severe consumption of the donor materials. For the development of approaches that are utilized to produce functional semiconducting microribbons, important considerations include: i) large-scale production in a convenient manner that without involving the complex and precise fabrication process; ii) capable of deterministically assembling the obtained semiconducting microribbons; iii) cyclic use of the donor materials to reduce the costs.

Here, we propose a matryoshka-inspired approach for continuous production and deterministic assembly of flexible silicon microribbons (SiMRs) and electronic devices via selective transfer printing. The obtained SiMRs from the donor silicon-on-insulator (SOI) exactly maintain the alignment of the pre-defined pattern through the anchoring effect of the partly etched buried silicon dioxide edge. Repeating the processing loop of "wet etch-selective transfer-printing" leads to the large-scale and repeatable production of SiMRs on desired substrates, as well as the cyclic use of the donor SOI. Both experimental and theoretical investigations are performed to optimize the surface morphology of polydimethylsiloxane (PDMS) stamp, which strongly determines the selective transfer efficiency of SiMRs. Finally, the as-prepared SiMRs via the first and second processing loop are functionalized into photodetectors, as an example, which exhibit the similar optoelectronic responses. These presented results imply the capability of the proposed approach for preparing other flexible semiconducting microribbons, which can be integrated with metals, dielectrics, and patterns of dopants for high-performance flexible electronics. As a universal approach, the transfer printing technique involved in our research could maintain its advantages in the flexible or stretchable electronics, such as the assembly of heterogeneous materials/junctions [43,44], the fabrication of sensors or circuits on three-dimensional curved surfaces [45], the integration of various functional devices to form a standalone stretchable sensing platform [46], and other related.

2. Experimental section

2.1. Selective transfer printing of SiMRs

Thin SiMRs (about 1 μm in width) were prepared from commercial (100) SOI wafers (top silicon: 20 nm and buried oxide: 150 nm). First, SOI wafer was ultrasonically cleaned with acetone, ethanol, and deionized water. Then, photoresist (AZ-5214) was spin-coated on cleaned SOI wafer with a speed of 4000 rpm for 30 s. After the exposure by conventional photolithography and development, reactive ion etching was used to define the pattern on SOI by O_2/SF_6 (3/15 sccm) for 40 s at a pressure of 100 mTorr. The patterned SOI wafer was then immersed in HF solution (5%) for 15 min to partially remove the buried oxide layer, and suspended SiMRs (about 1 μm in width) were emerged at the edge of patterns. A viscoelastic stamp was used to selective transfer printing of these SiMRs to target substrates. PDMS (Sylgard-184, Dow Corning, thickness ~2 mm) slabs were prepared by mixing base A and curing agent B with a weight ratio of 10:1, which was cured at 70 °C for 2 h. The stamp was put conformal contact against the wet etched SOI wafer with suspended SiMRs, then peeling-off the stamp a speed of about 10 cm/s completed the selective transfer of SiMRs. The transferred SiMRs were then put on the target substrate with a half-cured SU-8 2002 adhesion layer (spin coating at 4000 rpm for 30 s, annealed at 65 °C for 2 min). After full curing SU-8 adhesion layer (annealed at 90 °C for 2 min, exposure for 5 min using a general ultraviolet lamp), the stamp was peeled up slowly (at a speed of about 1 mm/s) from the substrate to complete the printing of SiMRs.

2.2. Fabrication of grating PDMS stamp

Grating PDMS stamps were prepared on by casting and curing the precursor against Si wafer with a grating surface. The grating Si wafer contains periodic groove and protuberance on the surface, with the period, or total width, of 10 μm. After mixing base A and curing agent B with a weight ratio of 10:1, the mixture was poured onto the grating Si wafer. Curing the mixture at 70 °C for 2 h and peeling off from the grating Si wafer can obtain the grating PDMS stamp. Grating Si wafers were fabricated through photolithography and dry etch. For the optimization of grating PDMS stamps, a set of groove widths, including 2 μm, 3 μm, 4 μm, and a set of groove depths, including 100 nm, 200 nm, 300 nm, 400 nm, 500 nm, 700 nm, were prepared.

2.3. Fabrication of SiMR-based NPN photodetector

A slightly boron-doped p-type SOI wafer (top silicon: 220 nm and buried oxide: 2 μm) was patterned into square (side length: 60 μm) array through photolithography and dry etch processes. Then, silicon dioxide layer with a thickness of 600 nm was deposited as the barrier layer for the following doping. Photolithography and etching processes defined the doping window. Phosphorus-based spin-on-dopant was spin-coated on the sample at a speed of 3000 rmp for 30 s. After annealing at 1000 °C for 15 min in a nitrogen condition, the residues were removed by HF. Immersing the sample in 5% HF formed the suspended NPN SiMRs, and the wet etch time was optimized to control their width. Then, the suspended NPN SiMRs were assembled on SU-8/Si substrates via the selective transfer printing. Cr/Au (10 nm/30 nm) electrodes were deposited by electron beam evaporation. Notably, repeating the selective transfer printing, matryoshka-like SiMR-based NPN photodetectors were fabricated. The time consumption in fabricating flexible SiMR array using the proposed selective transfer printing approach is significantly shorter than that using traditional approach, especially for the second and more fabrication loops, as estimated in the Supporting information.

2.4. Characterizations

Morphologies of SOI patterns and transferred SiMR arrays were characterized with an optical microscope (OLYMPUS BX51) and a scanning electron microscope (SEM, Zeiss Sigma). Optoelectronic characterizations were carried out using a probe station equipped with a precision source/measure unit (Keysight B2902B) at room temperature and an excitation laser. The wavelength of the excitation laser was 450 nm, and the square wave (0.5 Hz, 4 Vpp) was achieved through a waveform generator (Keysight 33500B) for transient optoelectronic response tests. The light intensity was tested using an optical power meter (Thorlabs S130C).

2.5. Finite element analysis

Finite element analysis was used to study the stress distribution and contact area for grating PDMS stamp with different geometrical parameters. The simulation was performed by the commercial software ABAQUS with a simplified two-dimensional model. Both PDMS and Si were simplified as isotropic and linear elastic body, because only the mechanical deformation and the stress distribution which mainly caused by the elasticity of PDMS stamps are investigated in the simulation. At the interface, the PDMS surface was considered the slave surface while the rigid surface (Si surface) was considered the master one. The Surface-to-Surface scheme was used. The mesh type both PDMS and Si was free quad-dominated. The load type was a uniform stress. The mechanical parameters of PDMS are referred to in previous literature [47].

3. Results and discussions

Matryoshka dolls are known as a set of dolls with similar shape but gradually decreased size nested one inside another, as schematically shown in Fig. 1A. Inspired by matryoshka dolls, continuous production of the flexible SiMR array is achieved by repeating the selective transfer printing, as displayed in Fig. 1B. As a result, multiple SiMR-based electronic device arrays with the same function are available after a single pre-doping process. The selective transfer printing of SiMRs is illustrated in Fig. 1C. Starting with a cleaned SOI wafer, the successive photolithography, dry etching, and selective doping processes induce pattering and doping of top silicon nanomembranes (SiNMs). Immersing the patterned SOI into wet etchant and controlling the etching time can partly remove the buried oxide layer, forming the suspended SiMRs which exactly maintain the pre-defined order through the anchoring effect by left oxide edge. After conformal contact and peeling-off of the PDMS stamp, the suspended SiMRs can be selectively transferred via the so-called edge-cutting process [48]. Finally, the obtained flexible SiMRs are printing on desired substrate (herein, SU-8/Si substrate, or other substrates as shown in Fig. S1) for the following device fabrication.

Fig. 1D shows the optical microscopy images of the multiply prepared flexible SiMRs on PDMS through three times repeating the selective transfer printing, and the remaining SOI is shown in the right of Fig. 1D. Fabrication of other complex structures, consisted with SiMRs, such as stars (Fig. 1E), circles, crosses, ovals and alphabets (Fig. S2) are also available and repeatable by this matryoshka-inspired assembly method. The uniformity of transferred SiMRs over large areas across multiple peeling steps is shown in Fig. S3. The precise control and reproducibility of SiMR dimensions across different peeling cycles is shown in Fig. S4. Since the pattern definition is accomplished by a laboratory level ultra-violet lithography, large-area production of flexible SiMRs is convenient, as shown in Fig. 1F with a 1 cm × 1 cm assembled SiMR array on PDMS. Notably, the width of the obtained SiMR can be simply controlled by tuning the wet etching time (Fig. S5), which is also much smaller than the resolution limit (about 2 μm) of our

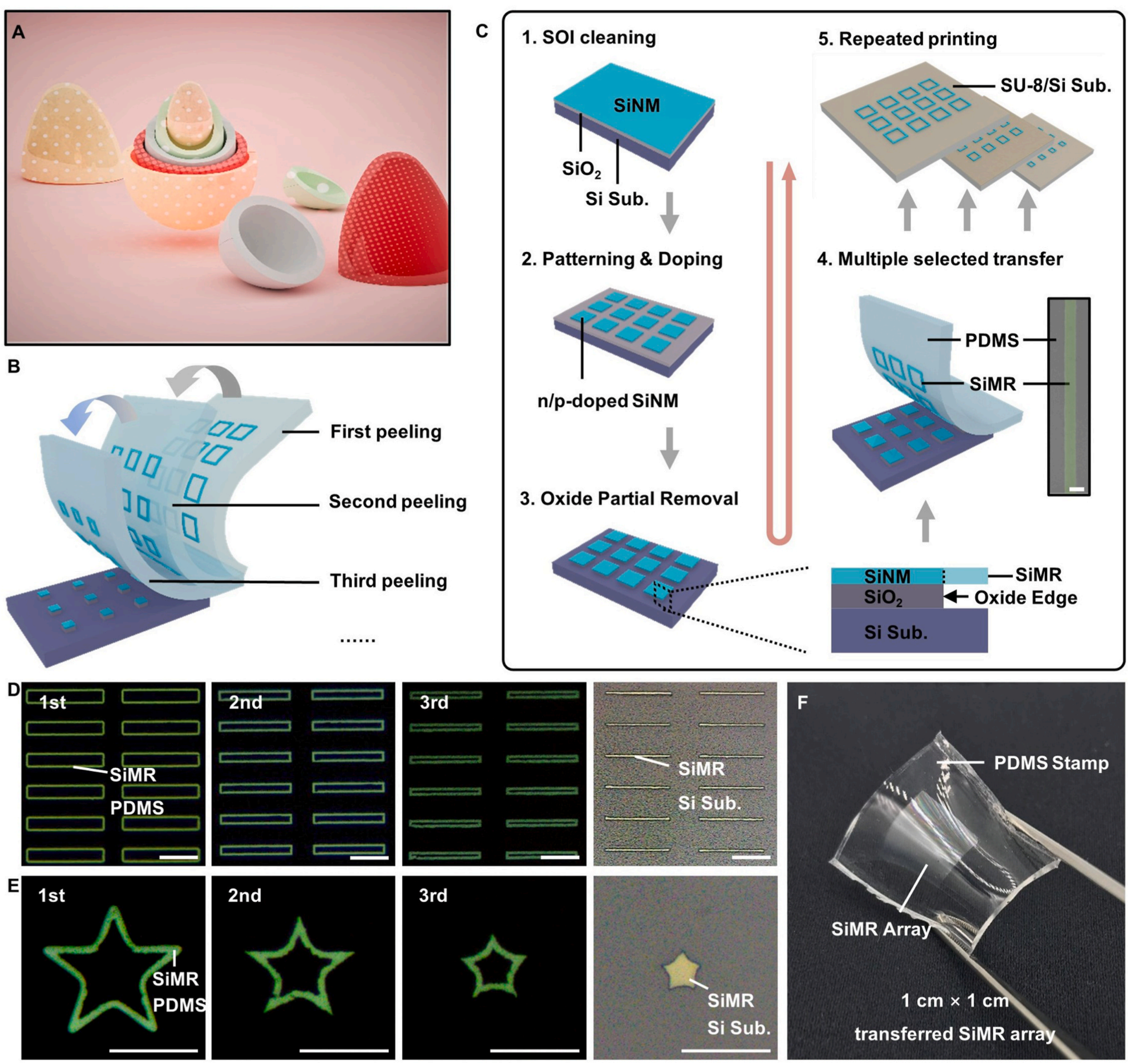

Fig. 1. (A) Schematic illustration of the layer-by-layer separate mode of a matryoshka doll. (B) Schematic illustration of the matryoshka inspired continuous assembly of SiMR arrays. (C) Schematic illustration of the selective transfer printing process of SiMRs, and the right of step 4 shows a SEM image of a typical transferred SiMR on the even PDMS stamp. The scale bar is 1 μm. Optical microscope images of the first, second, third peeling of the SiMR array and the remaining SOI pattern with: (D) stripe, and (E) star shape. All scale bars are 25 μm. (F) Optical image of a large-area (1 cm × 1 cm) SiMR array selectively transferred on PDMS stamp with a grating structure.

utilized photolithography, as demonstrated in the inset of Fig. 1C.

The production efficiency of SiMRs is strongly depended on the competition between the adhesive energy of PDMS/SiMR and the atomic bond energy inside silicon crystal for the selective transfer process, and on the competition between the adhesive energies of PDMS/SiMR and SiMR/substrate for the printing process. Since the Si–Si bond energy (222 kJ/mol [49,50]) and SiMR/substrate adhesive energy (determined by the Van der Waals force [51]) are relatively constant, the production efficiency of SiMRs can be, therefore, optimized by tuning the adhesive energy of PDMS/SiMR, which should be larger enough to break the Si–Si bond during the peeling-off, and be small enough for the release on target substrates. In this case, microstructured PDMS stamp with grating surface is designed, as shown in Fig. 2A. The even PDMS stamp with a flat surface is prepared for comparation, as shown in Fig. 2B. Switchable surface adhesion energy of PDMS/Si is realized by the change of contact area between PDMS and Si, which is induced by inflicting and releasing the external pressure on viscoelastic PDMS [52], as schematically shown in Fig. 2C. Optical microscope images of the selectively transferred SiMRs by using even and grating PDMS stamps are shown in Fig. 2D and E, respectively. Obvious enhancement in the transfer efficiency of SiMRs is obtained when utilizing the grating structured PDMS stamp. A scanning electron microscope (SEM) image of the transferred SiMR appears in Fig. 2F, in which the transferred SiMR suspends on the groove with a reduced contact area with PDMS, thus facilitating the following printing process on desired substrates.

To investigate the reasons for the enhanced transfer efficiency by using a grating structured PDMS stamp, both theoretical and finite element analyses are performed. Detailed calculations about the relationship between the contact area of PDMS/Si interface and the adhesive energy can be found in the Supporting Information. Briefly, for an even stamp, the energy release rate G can be calculated based on the elastomeric model [52,53], $G = \frac{F}{w}$, where F is the peeling force normal to the interface, w is the width of the stamp. The parameters and their denotations are schematically defined in Fig. S6. The transfer process by using an even stamp is realized by comparing the critical energy release rate, i.e.,

$$G_{crit}^{film/substrate} < G_{crit}^{stamp/film} \tag{1}$$

where $G_{crit}^{film/substrate}$ and $G_{crit}^{stamp/film}$ denote the critical energy release rate for the film/substrate and stamp/film interface during transfer and printing, respectively. For the designed stamp with a grating surface, the corresponding critical energy release rate for printing is modified as $\alpha G_{crit}^{stamp/film}$, where α is a coefficient depended on the geometry and applied pressure of the grating PDMS stamp. The parameters and their denotations, in this case, are schematically defined in Fig. S7. Therefore, to realize the transfer process by using the grating PDMS stamp, the following relationship should be satisfied, i.e.,

$$G_{crit}^{film/substrate} < \alpha G_{crit}^{stamp/film} \tag{2}$$

Since α is always smaller than 1 (see calculations in the Supporting Information), which means the contact area of grating PDMS/Si is always smaller than that of even PDMS/Si. At the same peeling velocity, critical energy release rate for the cases of using grating and even stamps are compared as,

$$\alpha G_{crit}^{stamp/film} < G_{crit}^{stamp/film} \tag{3}$$

From Equation (3), the critical energy release rate for the case of using an even stamp is always larger than that of using a grating stamp. Therefore, the elastomeric model alone cannot explain the results presented in Fig. 2D and E. Notably, an external pressure that opposites with the peeling force direction is applied to induce collapse of the grating PDMS stamp. Since PDMS is actually viscoelastic, the applied external pressure can affect the interface stress between PDMS and the underneath silicon or devices [54]. In this case, finite element analysis is performed with a simplified 2D model. The key geometry parameters and the stress distribution and deformation of the PDMS stamp appear in Fig. 3A. The width and height of protuberant parts are named as a and h, respectively, with a spacing of d. When a uniform vertical pressure is applied to the pre-contacted stamp, the middle part of the groove collapses to contact with the underneath Si. Nevertheless, the contact area of the grating PDMS/Si is smaller than that of the even PDMS/Si, but

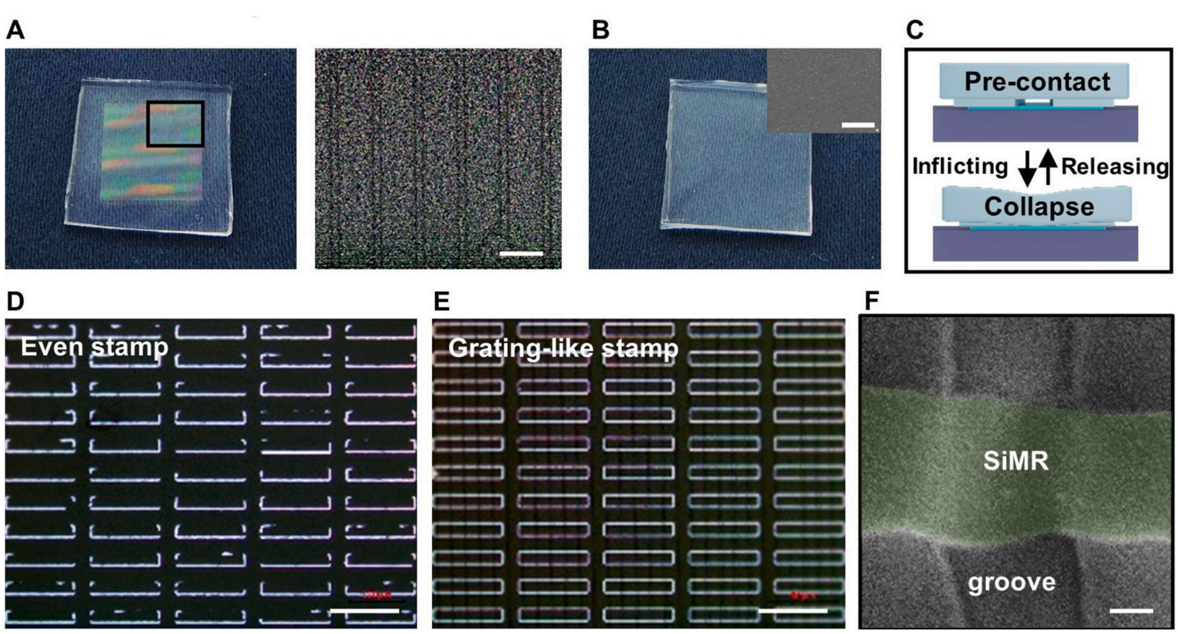

Fig. 2. (A) Optical image (left) and optical microscope image (right) of a grating PDMS stamp, and the scale bar is 10 μm. (B) Optical image of an even PDMS stamp. The inset shows the SEM image of the stamp surface, and the scale bar is 10 μm. (C) Schematic illustration of the selective transfer printing process of SiMRs, and the right of step 4 shows a SEM image of a typical transferred SiMR on the even PDMS stamp. The scale bar is 1 μm. Optical microscope images of the transferred SiMR using: (D) even stamp and (E) grating stamp, and all scale bars are 100 μm. (F) SEM image of a typical transferred SiMR suspended on grating PDMS stamp. The scale bar is 500 nm.

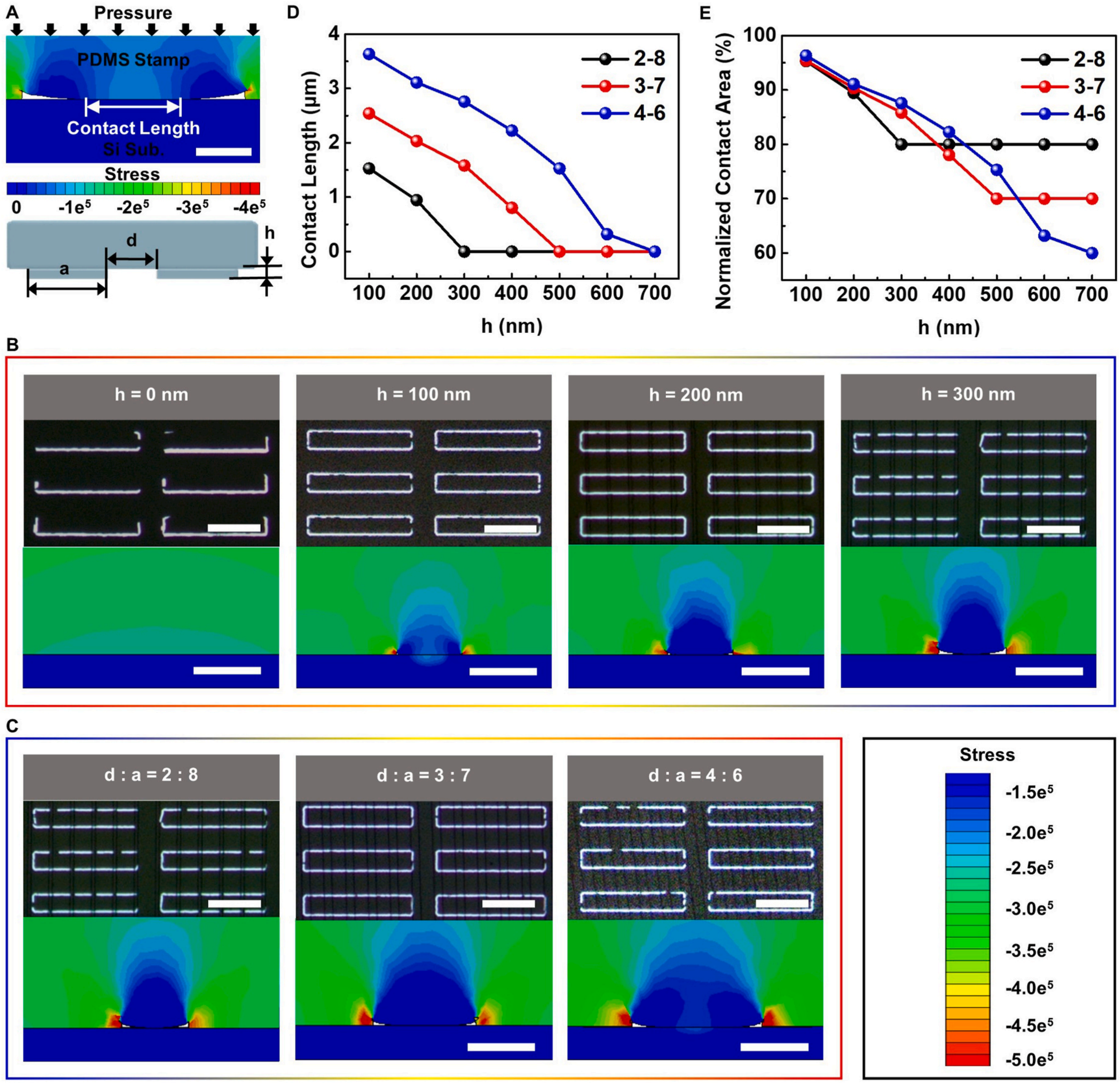

Fig. 3. (A) Simulated results of the deformation (or collapse) and stress distribution of a grating PDMS stamp induced by an external pressure with a scale bar of 500 nm, and the concept constant is highlighted. Parameters and symbols of the grating PDMS stamp are shown in the bottom. (B) Experimental results (top panels) of the variations of transfer efficiency with h (Scales bars: 25 μm), and simulated results (bottom panels) of the variations of stress distribution with h. For all cases, d/a is fixed as 2/8 (Scales bars: 2 μm). (C) Experimental results (top panels) of the variations of transfer efficiency with d/a (Scales bars: 25 μm), and simulated results (bottom panels) of the variations of stress distribution with d/a. For all cases, h is fixed as 300 nm (Scales bars: 2 μm). (D) The relationship between contact length and h with different values of d/a. (E) The relationship between nomarlized contact area and h with different values of d/a.

resulting in much larger pressure under the same external pressure. This large pressure leads to an increased peeling-off force of grating PDMS stamp, which contributes to the energy release rate during the transfer printing [54]. Therefore, the enhanced transfer efficiency of SiMRs by utilizing the grating PDMS stamp (98.5% when d/a = 2/8, h = 100 nm) compared to that with the even PDMS stamp (48.5%) can be attributed to the synergistic effect of contact area and interface stress.

Optimizations on the geometry (including h and d/a) of the designed grating stamp are conducted. Fig. 3B and C presents represented experimental and simulated results by using several grating stamps with different values of h and d/a. More detailed results can be found in Fig. S8. Fig. 3D and E summarized the contact area varying with h and d/a. For a fixed d/a (e.g., 2/8), as shown in Fig. 3B, variations in the value of h lead to heterogeneous stress distribution at the interface. Define the PDMS/Si contact before external pressure applied as the pre-contact. Simulation results in Fig. 3B show the deformation of PDMS stamp and the interface stress distribution under a constant external pressure. d/a is fixed as 2/8 for all cases. For an even stamp (h = 0 nm), although complete contact with the underneath Si can be realized, stress at the interface of PDMS/Si is small. Previous report has demonstrated that greater interface stress will result in a better PDMS/Si interface adhesion [54]. Therefore, uncomplete transfer of SiMRs (see the experimental results) appears in this case. For a grating PDMS stamp, the interface stress is much larger than that of an even stamp. However, the deformation of grating stamp with overlarge h (e.g., 300 nm) is unable to provide good contact with the underneath Si, as shown in Fig. 3D and E with black dots, thus inducing a dash-like SiMRs after the transfer (see the experimental results). Fig. 3C provides the optimization of d/a, while h is fixed as 300 nm. When d/a is small (for example, 2/8), although the interface stress is large (see the left-bottom panel of Fig. 3C), the deformation of groove is unable to provide good contact with the underneath Si (see the simulation result in Fig. 3D), so the transferred SiMRs are dash-like (see the experimental results). When d/a is large (for example, 4/6), although good contact with the underneath

Si occurs (see the simulation result in Fig. 3D), incomplete transfer of SiMRs is obtained from the experimental results, which is caused by the reduced interface stress (see the right-bottom panel of Fig. 3C) compared to that of a small d/a value. According to the presented results, the optimized grating PDMS stamps (d/a = 2/8, h = 100 nm) are used in the following researches.

Since the proposed selective transfer printing technique can continuously assemble multiple SiMRs with similar structure, multiple electronic devices with the same function are expectable by controlling the pattern of dopants prior to the transfer. Herein, SiMR-based NPN photodetector is demonstrated as an example. Fig. 4A schematically illustrates the fabrication process. In this case, the SOI (1 cm × 1 cm) is pre-patterned into square (side length: 60 μm) array, and each defined square is pre-doped into NPN type. After two times of selective transfer printing, multiple functionalized NPN SiMR arrays can be deterministically assembled onto target substrates without internal strain, as demonstrated by the Raman results in Fig. S9. Then, the following metallization process yields matryoshka-like SiMR-based NPN photodetectors, named as first-peeling photodetector, and second-peeling photodetector.

Fig. 4Bshows the I–V characteristics of the first-peeling photodetector under an illumination of a 450 nm laser with different power densities. Significant enhancement in photocurrent with the increase of the illuminated light power density is observed. To reveal the responsivity, photocurrent density defined as $(I_{on} - I_{off})/S$, where I_{on} and I_{off} are the measured current at light-on and light-off conditions, respectively, S is the device area is extracted. Fig. 4C presents a good linear relationship, with a linearity (R^2) of 0.997, between photocurrent density and power density. And the responsivity is calculated as 24.325 mA/W. A decrease in the responsivity (7.392 mA/W) of the second-peeling photodetector is obtained, as shown in Fig. 4E and F, which can be attributed to the shrinkage in the contact area between electrodes and SiMRs with different rounds of selective transfer printing. The difference in the responsivity between the first-peeling photodetector and the second-peeling photodetector can be significantly reduced by optimizing the structure design of electrodes, as shown in Fig. S10, where the contact area between electrodes and SiMRs maintain the same. Transient optoelectronic responses of first-peeling and second-peeling photodetectors to a pulsed light irradiation with varying power densities are presented in Fig. 4D and G, respectively, which exhibiting quick and stable optoelectronic responses. The response time reaches about 50 ms, as shown in Fig. S11. The matryoshka-inspired photodetector shows comparable responsivity and fast response time with recent reported literature [55–57]. More detailed performances about photocurrent, responsivity, and detectivity varying with the wavelength (from 300 nm to 1000 nm) of incident light can be found in Figs. S12 and S13. These demonstrated results imply the convenience and potential of the proposed approach for the large-scale production of flexible SiMRs and electronic devices.

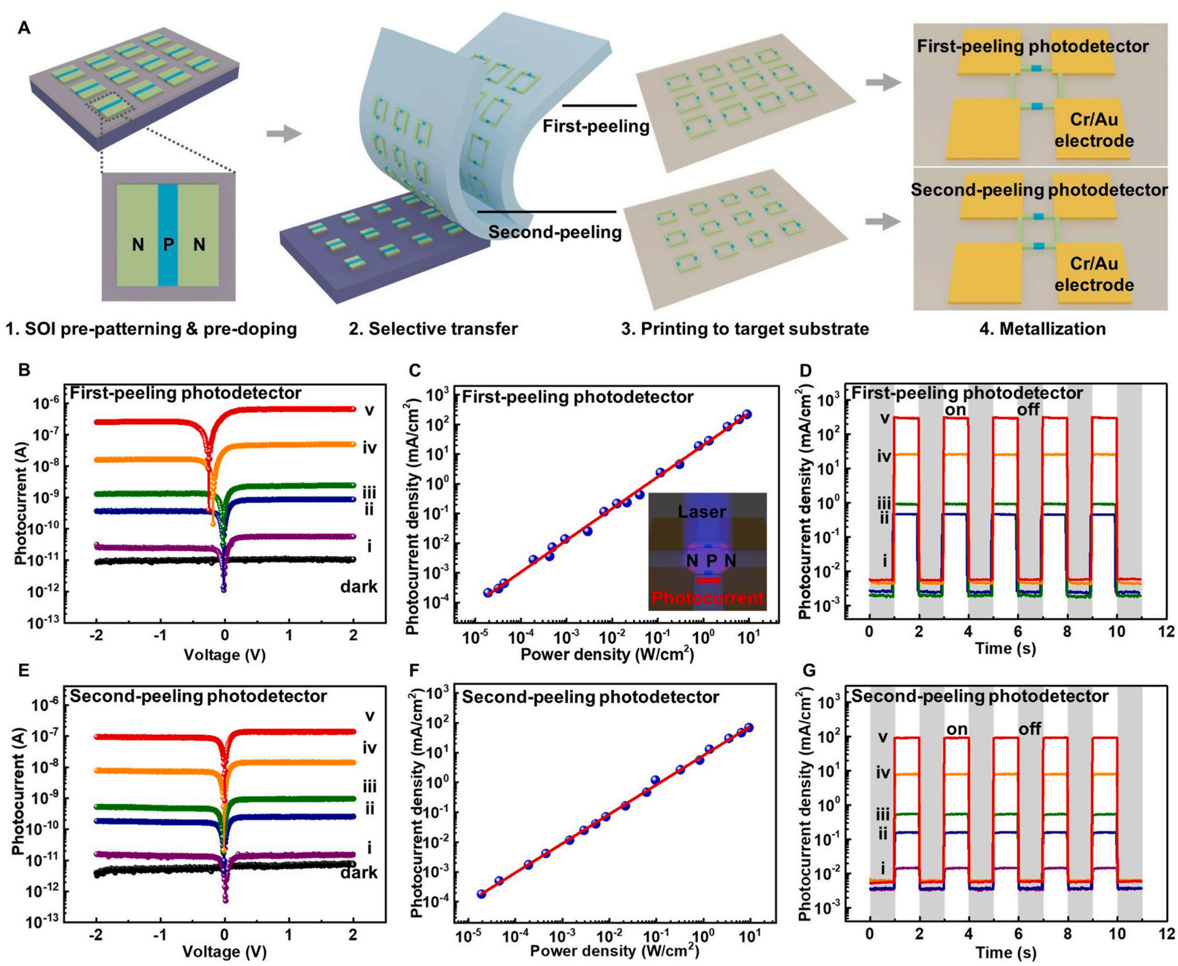

Fig. 4. (A) Schematic illustration of the fabrication of matryoshka-like SiMR-based NPN photodetectors. Optoelectronic charactorizations on the first-peeling photodetector: (B) I–V characteristics in response to a 450 nm laser with different power densities, (C) photocurrent density varying with the power density, (D) transient optoelectronic response to a pulsed light irridiation with h different power densities. Optoelectronic charactorizations on the second-peeling photodetector: (E) I–V characteristics in response to a 450 nm laser with different power densities, (F) photocurrent density varying with the power density, (G) transient optoelectronic response to a pulsed light irridiation with h different power densities.

4. Conclusion

In summary, inspired by the famous matryoshka doll, we developed a convenient approach to continuously assemble flexible SiMRs and photodetectors via selective transfer printing. Scalable productions of SiMR array with similar geometry and alignment and SiMR-based electronic device with the same function are realized by repeating the selective transfer printing. Experiments, theoretical analyses, and simulations demonstrate that utilizing a grating PDMS stamp can provide large adhesive energy during the selective transfer process. Optimizations about the geometry of grating PDMS stamp are performed, and the synergistic effect of contact area and interface stress offered by grating PDMS stamp induces an enhanced transfer efficiency of SiMRs. Finally, matryoshka-like flexible photodetectors, as an example, are fabricated by utilizing the sequentially prepared SiMRs. Photodetectors fabricated by the first and second round of selective transfer printing exhibit consistent and stable optoelectronic performances. These presented results demonstrate the capability of the developed approach for continuous, large-scale and deterministic assembly of flexible SiMRs, or other semiconducting microribbons, which can be integrated with metals, dielectrics, and patterns of dopants for high-performance electronics.

Credit author statement

Chunyan Qu: Investigation; Methodology; Roles/Writing – original draft; Qinglei Guo: Conceptualization; Supervision; Funding acquisition; Writing – review & editing. Xiaozhong Wu: Investigation; Resources. Chunyu You: Investigation. Binbin Wu: Investigation. Ziyu Zhang: Investigation. Yongfeng Mei: Conceptualization; Supervision; Funding acquisition; Writing – review & editing.

Declaration of competing interest

The authors declare that they have no known competing financial interests or personal relationships that could have appeared to influence the work reported in this paper.

Data availability

Data will be made available on request.

Acknowledgments

This work was supported by the National Key Technologies R&D Program of China [2021YFE0191800]; the National Natural Science Foundation of China [61975035, 51961145108]; the Science and Technology Commission of Shanghai Municipality [21142200200, 20501130700]; the Qilu Young Scholar Program of Shandong University; the Natural Science Foundation of Shandong Province in China [grant no. ZR2021MF008]; and the Shandong University Multidisciplinary Research and Innovation Team of Young Scholars [grant no. 2020QNQT015].

Appendix A. Supplementary data

Supplementary data to this article can be found online at https://doi.org/10.1016/j.mtphys.2023.101090.

References

[1] K.Q. Liu, S. Gao, Z. Zheng, X.L. Deng, S. Mukherjee, S.S. Wang, H. Xu, J.Q. Wang, J. F. Liu, T.Y. Zhai, Y. Fang, Spatially confined growth of fullerene to super-long crystalline fibers in supramolecular gels for high-performance photodetector, Adv. Mater. 31 (2019): 1808254.
[2] M.F. Peng, Z. Wen, X.H. Sun, Recent progress of flexible photodetectors based on low-dimensional II-VI semiconductors and their application in wearable electronics, Adv. Funct. Mater. (2022): 2211548.
[3] N. Ilyas, J.Y. Wang, C.M. Li, D.Y. Li, H. Fu, D.E. Gu, X.D. Jiang, F.C. Liu, Y.D. Jiang, W. Li, Nanostructured materials and architectures for advanced optoelectronic synaptic devices, Adv. Funct. Mater. 32 (2022): 2110976.
[4] A. Paghi, S. Mariani, G. Barillaro, 1D and 2D field effect transistors in gas sensing: a comprehensive review, Small (2023): 2206100.
[5] X. Zhang, J. Grajal, J. Luis Vazquez-Roy, U. Radhakrishna, X. Wang, W. Chern, L. Zhou, Y. Lin, P.-C. Shen, X. Ji, X. Ling, A. Zubair, Y. Zhang, H. Wang, M. Dubey, J. Kong, M. Dresselhaus, T. Palacios, Two-dimensional MoS2-enabled flexible rectenna for Wi-Fi-band wireless energy harvesting, Nature 566 (2019) 368–372.
[6] X. Li, C. Cao, C. Liu, W. He, K. Wu, Y. Wang, B. Xu, Z. Tian, E. Song, J. Cui, G. Huang, C. Zheng, Z. Di, X. Cao, Y. Mei, Self-rolling of vanadium dioxide nanomembranes for enhanced multi-level solar modulation, Nat. Commun. 13 (2022) 7819.
[7] J.A. Rogers, M.G. Lagally, R.G. Nuzzo, Synthesis, assembly and applications of semiconductor nanomembranes, Nature 477 (2011) 45–53.
[8] G.S. Huang, Y.F. Mei, Assembly and self-assembly of nanomembrane materials-from 2D to 3D, Small 14 (2018): 1703665.
[9] Y. Kim, J.M. Suh, J. Shin, Y. Liu, H. Yeon, K. Qiao, H.S. Kum, C. Kim, H.E. Lee, C. Choi, H. Kim, D. Lee, J. Lee, J.H. Kang, B.I. Park, S. Kang, J. Kim, S. Kim, J. A. Perozek, K. Wang, Y. Park, K. Kishen, L. Kong, T. Palacios, J. Park, M.C. Park, H. J. Kim, Y.S. Lee, K. Lee, S.H. Bae, W. Kong, J. Han, J. Kim, Chip-less wireless electronic skins by remote epitaxial freestanding compound semiconductors, Science 377 (2022) 859–869.
[10] X.L. Zhang, H.H. Huang, L.J. Jin, C. Wen, Q. Zhao, C.Y. Zhao, J.J. Guo, C. Cheng, H.S. Wang, L. Zhang, Y.Y. Li, Y.M. Maung, J.Y. Yuan, W.L. Ma, Ligand-assisted coupling manipulation for efficient and stable FAPbI(3) colloidal quantum dot solar cells, Angew. Chem.-Int. Edit. 62 (2022): e2022142.
[11] X.Z. Xu, B.J. Bowen, R.E.A. Gwyther, M. Freeley, B. Grigorenko, A.V. Nemukhin, J. Eklof-Osterberg, K. Moth-Poulsen, D.D. Jones, M. Palma, Tuning electrostatic gating of semiconducting carbon nanotubes by controlling protein orientation in biosensing devices, Angew. Chem.-Int. Edit. 60 (2021) 20184–20189.
[12] K. Peng, D. Jevtics, F.L. Zhang, S. Sterzl, D.A. Damry, M.U. Rothmann, B. Guilhabert, M.J. Strain, H.H. Tan, L.M. Herz, L. Fu, M.D. Dawson, A. Hurtado, C. Jagadish, M.B. Johnston, Three-dimensional cross-nanowire networks recover full terahertz state, Science 368 (2020) 510–513.
[13] C.J. Wu, J. Dai, X.F. Li, L. Gao, J.Z. Wang, J. Liu, J. Zheng, X.J. Zhan, J.W. Chen, X. Cheng, M.C. Yang, J.Y. Tang, Ion-exchange enabled synthetic swarm, Nat. Nanotechnol. 16 (2021) 288–295.
[14] A. Aljarb, J.H. Fu, C.C. Hsu, C.P. Chuu, Y. Wan, M. Hakami, D.R. Naphade, E. Yengel, C.J. Lee, S. Brems, T.A. Chen, M.Y. Li, S.H. Bae, W.T. Hsu, Z. Cao, R. Albaridy, S. Lopatin, W.H. Chang, T.D. Anthopoulos, J. Kim, L.J. Li, V. Tung, Ledge-directed epitaxy of continuously self-aligned single-crystalline nanoribbons of transition metal dichalcogenides, Nat. Mater. 19 (2020) 1300–1306.
[15] C.H. Wang, X.Y. Xu, X.D. Pi, M.D. Butala, W. Huang, L. Yin, W.B. Peng, M. Ali, S. C. Bodepudi, S. Qiao, Y. Xu, W. Sun, D.R. Yang, Neuromorphic device based on silicon nanosheets, Nat. Commun. 13 (2022) 5216.
[16] C.H. Xu, X. Wu, G.S. Huang, Y.F. Mei, Rolled-up nanotechnology: materials issue and geometry capability, Adv. Mater. Technol. 4 (2019): 1800486.
[17] Z. Liu, W.D. Qiu, X.M. Peng, G.W. Sun, X.Y. Liu, D.H. Liu, Z.C. Li, F.R. He, C. Y. Shen, Q. Gu, F.L. Ma, L. Yip, L.T. Hou, Z.J. Qi, S.J. Su, Perovskite light-emitting diodes with EQE exceeding 28% through a synergetic dual-additive strategy for defect passivation and nanostructure regulation, Adv. Mater. 33 (2021): 2103268.
[18] A. Zumeit, A.S. Dahiya, A. Christou, D. Shakthivel, R. Dahiya, Direct roll transfer printed silicon nanoribbon arrays based high-performance flexible electronics, NPJ Flex. Electron. 5 (2021) 18.
[19] S.N. Chen, X.Y. Ma, Z.R. Cai, H.R. Long, X.Y. Wang, Z. Li, Z.Y. Qu, F.J. Zhang, Y. L. Qiao, Y.L. Song, A direct writing approach for organic semiconductor single-crystal patterns with unique orientation, Adv. Mater. 34 (2022): 2200928.
[20] A. Zumeit, A.S. Dahiya, A. Christou, R. Mukherjee, R. Dahiya, Printed gaas microstructures-based flexible high-performance broadband photodetectors, Adv. Mater. Technol. 7 (2022): 2200772.
[21] C.Z. Zhao, Q.Z. Liu, K.M. Cheung, W.F. Liu, Q. Yang, X.B. Xu, T.X. Man, P.S. Weiss, C.W. Zhou, A.M. Andrews, Narrower nanoribbon biosensors fabricated by chemical lift-off lithography show higher sensitivity, ACS Nano 15 (2021) 904–915.
[22] C. Qu, Q. Guo, G. Huang, Y. Mei, Local cracking-induced scalable flexible silicon nanogaps for dynamically tunable surface enhanced Raman scattering substrates, Adv. Mater. Interfac. 8 (2021): 2100661.
[23] Q.Z. Liu, Y.H. Liu, F.Q. Wu, X. Cao, Z. Li, M. Alharbi, A.N. Abbas, M.R. Amer, C. W. Zhou, Highly sensitive and wearable In2O3 nanoribbon transistor biosensors with integrated on-chip gate for glucose monitoring in body fluids, ACS Nano 12 (2018) 1170–1178.
[24] X.L. Tong, Z.N. Tian, J.Y. Sun, V.C. Tung, R.B. Kaner, Y.L. Shao, Self-healing flexible/stretchable energy storage devices, Mater. Today Off. 44 (2021) 78–104.
[25] S. Shang, C. Du, Y. Liu, M. Liu, X. Wang, W. Gao, Y. Zou, J. Dong, Y. Liu, J. Chen, A one-dimensional conductive metal-organic framework with extended pi-d conjugated nanoribbon layers, Nat. Commun. 13 (2022) 7599.
[26] W. Deng, Y. Zhou, A. Libanori, G. Chen, W. Yang, J. Chen, Piezoelectric nanogenerators for personalized healthcare, Chem. Soc. Rev. 51 (2022) 3380–3435.
[27] B.R. Xu, X.Y. Lin, Y.F. Mei, Versatile rolling origami to fabricate functional and smart materials, Cell Rep. Phys. Sci. 1 (2020): 100244.
[28] H.B. Zhao, Y.J. Lee, M.D. Han, B.K. Sharma, X.X. Chen, J.H. Ahn, J.A. Rogers, Nanofabrication approaches for functional three-dimensional architectures, Nano Today 30 (2020): 100825.

[29] C. Liu, B. Yao, T.G. Dong, H.G. Ma, S.B. Zhang, J.Z. Wang, J. Xu, Y. Shi, K.J. Chen, L.B. Gao, L.W. Yu, Highly stretchable graphene nanoribbon springs by programmable nanowire lithography, NPJ 2D Mater. Appl. 3 (2019) 23.

[30] M. Sang, K. Kang, Y. Zhang, H.Z. Zhang, K. Kim, M. Cho, J. Shin, J.H. Hong, T. Kim, S.K. Lee, W.H. Yeo, J.W. Lee, T. Lee, B.X. Xu, K.J. Yu, Ultrahigh sensitive Au-doped silicon nanomembrane based wearable sensor arrays for continuous skin temperature monitoring with high precision, Adv. Mater. 34 (2022): 2105865.

[31] X. Li, J. Wang, One-dimensional and two-dimensional synergized nanostructures for high-performing energy storage and conversion, InfoMat 2 (2020) 3–32.

[32] J. Yao, H. Yan, C.M. Lieber, A nanoscale combing technique for the large-scale assembly of highly aligned nanowires, Nat. Nanotechnol. 8 (2013) 329–335.

[33] J.X. Lin, H.W. Hu, J. Luo, L. Miao, Z.H. Yang, M. Chen, M. Zhang, J.Z. Ou, Micro/nanoarrays and their applications in flexible sensors: a review, Mater. Today Nano 19 (2022): 100224.

[34] D. Chen, Y.M. Wang, H.L.Z. Zhou, Z.G. Huang, Y. Zhang, C.F. Guo, H.M. Zhou, Current and future trends for polymer micro/nanoprocessing in industrial applications, Adv. Mater. 34 (2022): 2200903.

[35] M.H. Seo, J.Y. Yoo, M.S. Jo, J.B. Yoon, Geometrically structured nanomaterials for nanosensors, NEMS, and nanosieves, Adv. Mater. 32 (2020): 1907082.

[36] I. Kim, J. Mun, K.M. Baek, M. Kim, C.L. Hao, C.W. Qiu, Y.S. Jung, J. Rho, Cascade domino lithography for extreme photon sequeezing, Mater. Today 39 (2020) 89–97.

[37] M. Chen, L. Pethoe, A.S. Sologubenko, H. Ma, J. Michler, R. Spolenak, J. M. Wheeler, Achieving micron-scale plasticity and theoretical strength in silicon, Nat. Commun. 11 (2020) 2681.

[38] M. Hollenbach, N. Klingner, N.S. Jagtap, L. Bischoff, C. Fowley, U. Kentsch, G. Hlawacek, A. Erbe, N.V. Abrosimov, M. Helm, Y. Berencen, G.V. Astakhov, Wafer-scale nanofabrication of telecom single-photon emitters in silicon, Nat. Commun. 13 (2022) 7683.

[39] L. Sun, H.L. Zou, S.B. Sang, A low-cost and high-efficiency method for four-inch silicon nano-mold by proximity uv exposure, Nanotechnology 33 (2022): 075303.

[40] S.V. Sreenivasan, Nanoimprint lithography steppers for volume fabrication of leading-edge semiconductor integrated circuits, Microsyst. Nanoeng. 3 (2017): 17075.

[41] Y. Meng, Y.Z. Chen, L.H. Lu, Y.M. Ding, A. Cusano, J.A. Fan, Q.M. Hu, K.Y. Wang, Z.W. Xie, Z.T. Liu, Y.M. Yang, Q. Liu, M.L. Gong, Q.R. Xiao, S.L. Sun, M.M. Zhang, X.C. Yuan, X.J. Ni, Optical meta-waveguides for integrated photonics and beyond, Light Sci. Appl. 10 (2021) 235.

[42] W.B. Jung, S. Jang, S.Y. Cho, H.J. Jeon, H.T. Jung, Recent progress in simple and cost-effective top-down lithography for approximate to 10 nm scale nanopatterns: from edge lithography to secondary sputtering lithography, Adv. Mater. 32 (2020): 1907101.

[43] H.L. Zhou, W.Y. Qin, Q.M. Yu, H.Y. Cheng, X.D. Yu, H.P. Wu, Transfer printing and its applications in flexible electronic devices, Nanomaterials 9 (2019) 283.

[44] Q.M. Yu, X.D. Yu, H.L. Zhou, F.R. Chen, H.Y. Cheng, Effects of material properties and geometric parameters on electromagnetic-assisted transfer printing, J. Phys. D Appl. Phys. 52 (2019): 255302.

[45] S.H. Zhang, J. Zhu, Y.Y. Zhang, Z.S. Chen, C.Y. Song, J.Q. Li, N. Yi, D.H. Qiu, K. Guo, C. Zhang, T.S. Pan, Y. Lin, H.L. Zhou, H. Long, H.B. Yang, H.Y. Cheng, Standalone stretchable RF systems based on asymmetric 3D microstrip antennas with on-body wireless communication and energy harvesting, Nano Energy 96 (2022): 107069.

[46] N. Yi, Y.Y. Gao, A.L.V. Jr, J. Zhu, D. Erdely, C. Xue, R. Lavelle, H.Y. Cheng, Fabricating functional circuits on 3D freeform surfaces via intense pulsed light-induced zinc mass transfer, Mater. Today 50 (2021) 24–34.

[47] F. Carrillo, S. Gupta, M. Balooch, S.J. Marshall, G.W. Marshall, L. Pruitt, C. M. Puttlitz, Nanoindentation of polydimethylsiloxane elastomers: effect of crosslinking, work of adhesion, and fluid environment on elastic modulus, J. Mater. Res. 20 (2005) 2820–2830.

[48] Q. Guo, M. Zhang, Z. Xue, G. Wang, D. Chen, R. Cao, G. Huang, Y. Mei, Z. Di, X. Wang, Deterministic assembly of flexible Si/Ge nanoribbons via edge-cutting transfer and printing for van der waals heterojunctions, Small 11 (2015) 4140–4148.

[49] J.E. Huheey, E.A. Keiter, R.L. Keiter, Appendix E: bond energies and bond lengths, in: Inorganic Chemistry: Principles of Structure and Reactivity, fourth ed., HarperCollins College publishers, New York, 1993, pp. A21–A34.

[50] G.X. Chen, S.B. Chen, Z.W. Lin, R. Huang, Y.Q. Guo, Enhanced red emission from amorphous silicon carbide films via nitrogen doping, Micromachines 13 (2022) 2043.

[51] C.H. Linghu, S. Zhang, C.J. Wang, J.Z. Song, Transfer printing techniques for flexible and stretchable inorganic electronics, NPJ Flex. Electron. 2 (2018) 26.

[52] X. Feng, M.A. Meitl, A.M. Bowen, Y. Huang, R.G. Nuzzo, J.A. Rogers, Competing fracture in kinetically controlled transfer printing, Langmuir 23 (2007) 12555–12560.

[53] K. Kendall, Thin-film peeling - elastic term, J. Phys. D Appl. Phys. 8 (1975) 1449–1452.

[54] C.M. Liang, F.J. Wang, Z.C. Huo, B.C. Shi, Y.L. Tian, X.Y. Zhao, D.W. Zhang, Pull-off force modeling and experimental study of PDMS stamp considering preload in micro transfer printing, Int. J. Solid Struct. 193 (2020) 134–140.

[55] M.J. Dang, H.-C. Yuan, Z.Q. Ma, J.G. Ma, G.X. Qin, The fabrication and characterization of flexible single-crystalline silicon and germanium p-intrinsic-n photodetectors on plastic substrates, Appl. Phys. Lett. 110 (2017): 253104.

[56] Y.L. Tang, J. Chen, High responsivity of Gr/n-Si Schottky junction near-infrared photodetector, Superlattice. Microst. 150 (2021): 106803.

[57] A.A. Ahmed, M.R. Hashim, T.F. Qahtan, M. Rashid, Preparation and characteristics study of self-powered and fast response p-NiO/n-Si heterojunction photodetector, Ceram. Int. 48 (14) (2022) 20078–20089.